# Efficient growth of sub-micrometric MOF crystals inside the channels of AAO membranes

Mahmoud Maksoud, Nans Roques, Stéphane Brandès, Laurent Arurault,

Jean-Pascal Sutter

# Efficient growth of sub-micrometric MOF crystals inside the channels of AAO membranes†

Mahmoud Maksoud,[ab] Nans Roques,*[ab] Stéphane Brandès,[c] Laurent Arurault[d] and Jean-Pascal Sutter*[ab]

A dynamic step-by-step methodology has been implemented to grow the HKUST-1 porous coordination polymer inside commercial anodic aluminium oxide membranes. Efficient crystal growth is achieved from the membrane inner walls and over the whole membrane thickness when copper acetate colloidal suspensions and benzene tricarboxylic acid solutions are forced to flow through the membrane. Sorption properties of the HKUST-1 embedded in membranes show selectivity for $CO_2$ over $CO$, $CH_4$, $O_2$ and $N_2$ similar to the bulk material.

## Introduction

Over the past fifteen years, Metal–Organic Frameworks (MOFs)[1] have drawn tremendous interest because of their potential applications in catalysis,[2,3] gas storage,[4] sensing,[5] drug delivery,[6] *etc.* Until 2005, research in this field was mainly focused on bulk crystals. Since the pioneering work of Fischer and coworkers,[7] who demonstrated the principles of bio-mineralization[8] to be adaptable to porous coordination polymer synthesis, numerous studies have been devoted to the controlled growth of such materials on various types of surfaces.[9,10] MOF-coatings have been achieved mainly with carboxylate- and imidazolate-based MOFs.[10] These have been obtained through the seeding of preformed MOF-nanoparticles,[11] "seeding and growth" approaches,[12] or using step-by-step methodologies (SBS, in the following) onto a range of surfaces such as bare metal oxides or appropriately terminated self-assembled monolayers (SAMs) grafted on gold, silicon or metal-oxides. The resulting materials were found to be efficient as sensors[13] and smart textiles,[14] in supported catalysis[15] and in membrane-based gas separation.[16]

Because MOFs are chemically and/or mechanically fragile, prone to attrition issues and aging, their embedding in a protecting shell such as an organic or inorganic matrix can be envisaged. Recent reports showed that the preparation of MOF-composites was possible from a wide range of organic polymers and metal-oxides such as macro/mesoporous silica or magnetic iron particles, among others.[17] MOF-composites of interest would also result from the selective filling of the channels of Anodized Aluminum Oxide (AAO) membranes. This possibility has been suggested in the seminal work of Fischer *et al.*[7] and constitutes a focus of particular interest for the fields of materials and molecular materials.[18,19] Herein, we show that the growth of sub-micrometric MOF crystals can be efficiently achieved from the inner walls of an AAO membrane. This proved quite facile for HKUST-1 by combining a dynamic SBS synthesis procedure with the use of colloidal suspensions of the metal ion precursor.

## Results and discussion

Commercial AAO (CAAO) membranes (Whatman Anodisc, pore diameter $\approx$ 0.2 μm) were deflected from their principal application (filtration) to be used as substrates.[20] Representative field-emission SEM (FESEM) images of both sides of these membranes are given in Fig. S1† as a reference. The OH-groups and/or metal sites located at the CAAO membrane surface were expected to allow the grafting and growth of the MOF material without the need of any surface activation/modification.[21] HKUST-1[22] was used as a MOF representative.

Several preparation procedures have been explored to achieve a selective and efficient load inside the membrane channels. The results obtained when a CAAO membrane was introduced into a solvothermal synthesis reaction mixture are shown in Fig. 1a–c, S2 and S3.† FESEM pictures reveal that both sides of the CAAO substrate are covered with a rather dense crystalline coating of HKUST-1. Crystal growth inside the channels is limited to the boundary of the membrane. Almost no crystals are found in the cross-section central region (Fig. 1b). The static SBS procedure, which aims at soaking the membrane alternately in $[Cu(OAc)_2]_2$ and benzene tricarboxylic

[a]CNRS, LCC (Laboratoire de Chimie de Coordination), 205 route de Narbonne, F-31077 Toulouse, France. E-mail: nans.roques@lcc-toulouse.fr; sutter@lcc-toulouse.fr

[b]Université de Toulouse, UPS, INPT, F-31077, Toulouse, France

[c]ICMUB (Institut de Chimie Moléculaire de l'Université de Bourgogne), UMR 6302 CNRS, Université de Bourgogne, 21078 Dijon, France
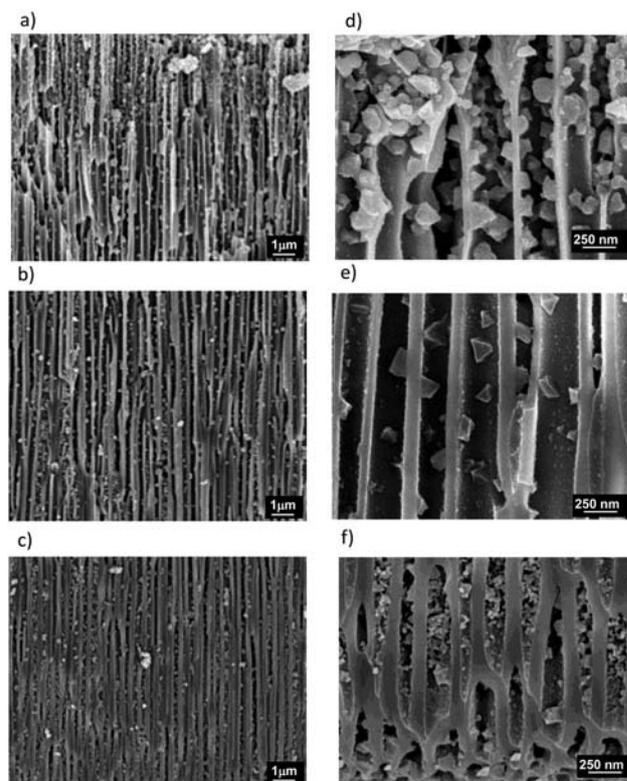
[d]Université de Toulouse, CIRIMAT, UPS/INPT/CNRS, LCMIE, 118 route de Narbonne, F-31062 Toulouse, France
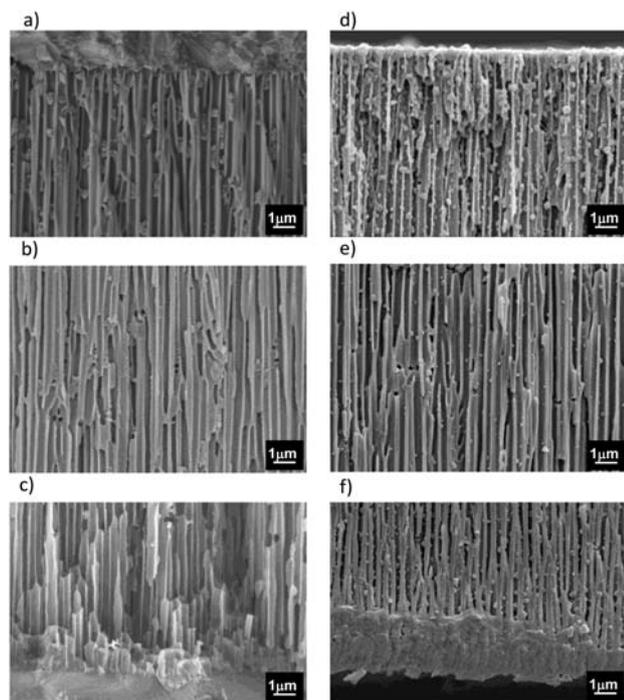
**Fig. 1** FESEM images of the cross-section of CAAO membranes after solvothermal synthesis (left column) and static SBS MOF synthesis (12 cycles, right column). (a) and (d) correspond to views close to side A; (b) and (e) correspond to views of the cross-section central region; and (c) and (f) correspond to views close to side B. Complementary information is supplied by Fig. S2, S3 and S4, S5,† respectively.
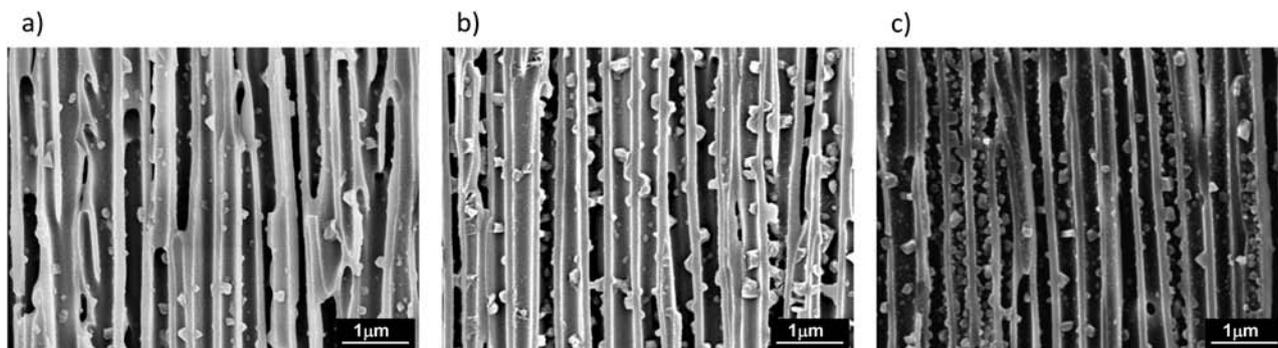


**Fig. 2** FESEM images of the cross-section of a metalized membrane after 12 cycles of dynamic SBS treatment. (a) View close to side A; (b) cross-section central region; and (c) view close to side B. Pictures (d)–(f) correspond to enlarged views of (a), (b), and (c), respectively. Complementary information is supplied by Fig. S7 and S8.†

acid (btc-$H_3$) absolute EtOH solutions, yielded MOF crystals all along the membrane channels. Nevertheless, examination of a membrane cross-section after 12 cycles reveals a much higher coverage near both sides of the membrane than in its central part (Fig. 1d–f, S4 and S5†). Furthermore, channel occlusion was observed after 24 cycles as a result of MOF crystal growth at the membrane external surface. To avoid occlusion of the channels by such a MOF-coating, the two sides (A and B) of the membranes were coated with ultrathin films of Pt (*ca.* 5 nm). These metal films are too thin to plug the pore entrance (Fig. S6†) but inhibit the coordination polymer grafting outside the pores. Reagent diffusion within the membrane channels was improved by performing the SBS procedure in a dynamic fashion, *i.e.* by flowing alternately [Cu(OAc)$_2$]$_2$ and btc-$H_3$ solutions through the channels, at a controlled rate. The results obtained after 12 cycles of dynamic SBS treatment of a metalized membrane are shown Fig. 2 and S7.† The load of HKUST-1 crystals all along the channels of the membrane is significantly increased. As expected, none are grafted to the metalized external sides (Fig. S8b†). The crystals in the channel sections close to side A are well shaped and notably larger (30 to 170 nm) than those found in the sections close to side B. Besides well shaped crystals, MOF-roughcast, with a grain size of a few nanometers, is also clearly observed on the channel walls of the central cross-section (Fig. 2e). Closer examination of the channels near side B further reveals the MOF nanoparticles to be interconnected to generate interstitial grain voids. The

difference in crystal growth might be attributed to a more turbulent flow of the reagent solutions close to the B end of the channels as a consequence of the reduced pore apertures (see Fig. S1b†).

IR and powder XRD measurements confirmed the formation of HKUST-1[22] (Fig. S9 and S10†). Incidentally, these two characterization techniques were also used to evidence the robustness of such composite membranes when exposed to air moisture for a long period of time. As can be seen in Fig. S11,† IR spectra registered for an as-synthesized composite membrane and for the same membrane being stored for 10 months in air are identical. PXRD measurements further reveal that the crystallinity of HKUST-1 is retained, and that no structural changes operate for the MOF crystals over this period.[23]

Interestingly, the amount of MOF loaded into the membrane channels can be tuned by the number of cycles applied. As an illustration, the results obtained after 2, 6, and 24 cycles of dynamic SBS treatment are shown in Fig. 3, which focuses on the cross-section central region of the corresponding membranes. HKUST-1 crystals are already observed over the whole channel length just after 2 cycles (Fig. 3a). Remarkably, the amount of crystals formed in the membrane's central part in this case is comparable to the one observed after 24 cycles using the classical SBS technique. Overall, the crystals' number and
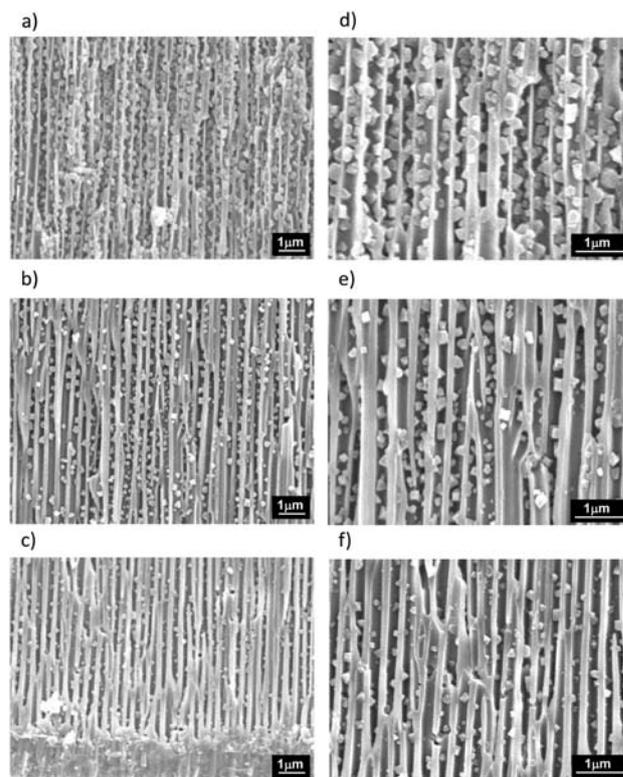
**Fig. 3** FESEM images of the cross-section central region of metalized membranes after 2 (a), 6 (b) and 24 cycles (c) of dynamic SBS treatment. Complementary information is supplied by Fig. S8.†

size clearly augment when the number of cycles is increased. When 24 cycles are realized, it can be noticed that some crystals have almost reached the crystal upper-size limit fixed by the channel section, and that some of the membrane channels are filled with MOF crystals. For the corresponding membranes, the average amount of MOF loaded in the channels is about 3–5 wt%. This value deduced from copper and carbon elemental analysis results (Table S1†) corresponds to 20–35% of the membrane void which is occupied by HKUST-1 crystals.

A significant improvement in the dynamic SBS procedure was observed when technical grade EtOH (containing 4% $H_2O$) was used as solvent instead of pure EtOH. For given flowing rates and concentrations, the MOF is formed more efficiently, and the size of the crystals can be controlled by changing the loading cycle duration as illustrated in Fig. S12.† Examination of a $10^{-3}$ M solution of $[Cu(OAc)_2]_2$ in 96% EtOH revealed the presence of nanoparticles, whose sizes were estimated to be 30–60 nm by dynamic light scattering (DLS, Fig. S13†). Seeding the membrane with such a colloidal suspension (Fig. S13b†) allows increasing the amount of $[Cu(OAc)_2]_2$ loaded in the channels during each cycle. When the membrane is subsequently reacted with btc-$H_3$, a significantly larger amount of coordination polymer is formed. The increase of the cycle duration also favors the formation of larger crystals. An optimized exposure time of the membrane to each reagent per cycle (60 minutes for $[Cu(OAc)_2]_2$ colloidal suspensions, and 120 minutes for the btc-$H_3$ solutions) has been deduced by following the area variation for characteristic IR bands during each step for two cycles (see Fig. S14†). A representative example of the membrane obtained after 2 cycles of dynamic SBS treatment using these conditions is shown in Fig. 4 and S15.† Overall, the MOF crystals formed in the channels are notably larger than those observed when absolute EtOH solutions are used. Most of them reach the upper size limit imposed by the channel dimensions (*i.e.* 0.2 μm). A larger amount of crystals is found close to side A compared to side B. This might be ascribed to a less efficient diffusion over the whole membrane thickness of the $[Cu(OAc)_2]_2$ particles for the second loading cycle due to the MOF crystals already present in the channels. Note that membranes are oriented to allow the reagent's flow to enter side A. This also explains why membrane occlusion is observed when a third load of $[Cu(OAc)_2]_2$ nanoparticles is operated. The average load of MOF

after just two cycles is comparable to that obtained after 24 cycles when absolute EtOH solutions are used. Remarkably, this procedure also reduces the time needed to prepare such MOF-loaded membranes from 36 h to 8 h. This synthetic approach was used to prepare the composite membranes engaged in sorption measurements.

Qualitative information confirming the HKUST-1 porosity is supplied by the color changes of the composite membranes associated with the MOF $H_2O$ release/adsorption (Fig. S16†). When they are heated or placed in a flow of dry gas (*e.g.* $N_2$),



**Fig. 4** FESEM images of the cross-section of a metalized membrane after 2 cycles of dynamic SBS treatment with $[Cu(OAc)_2]_2$ colloidal suspensions (60 minutes per cycle) and btc-$H_3$ solutions (120 minutes per cycle). (a) View close to side A; (b) cross-section central region; and (c) view close to side B. Pictures (d)–(f) correspond to enlarged views of (a), (b), and (c), respectively. Complementary information is supplied by Fig. S15.†

as-synthesized composite membranes turn dark blue, while the original light blue color is recovered upon standing the membranes in air at room temperature. These variations could be followed by IR (Fig. S16†). Quantitative information on adsorption properties of the composite membranes is supplied by $N_2$ adsorption isotherms recorded at 77 K for pristine CAAO membranes and for HKUST-1 loaded-membranes (Fig. 5). The alumina membranes are essentially macroporous, without any micropores. Large mesopores (up to >500 Å) are evidenced by $\alpha_s$-plot and BJH calculations. The total specific surface area is estimated to be 6.8 $m^2\ g^{-1}$ for these membranes. HKUST-1 containing membranes display a mixed type I/type II isotherm[24] because of the presence of both micro- and macropores in the corresponding composite material. Compared with the starting CAAO membranes, they exhibit a BET surface area that is increased to 50 $m^2\ g^{-1}$. The excess adsorption in the low pressure range originates exclusively from the micropores of the HKUST guest. The slight increase observed at high relative pressure with respect to the starting alumina membranes is ascribed to inter-crystal porosity.

The microporous surface is estimated to be 38 $m^2\ g^{-1}$ by the $\alpha_s$-plot (Fig. S17a†) for a microporous volume that represents 38% of the total porous volume (0.013 $cm^3\ g^{-1}$ vs. 0.034 $cm^3\ g^{-1}$, respectively). The coordination polymer pore size was obtained by plotting the $N_2$ sorption isotherm as a function of $\log(P/P_0)$, and analyzing the resulting curve using the Horvath–Kawazoe method (Fig. S17b†). In agreement with the presence of two inflection points observed in the low pressure region, a bimodal distribution of pores is obtained with pore dimensions close to 8 and 12 Å (Fig. S17c†). These results are in agreement with crystallographic data reported in the literature for HKUST-1.[22]

Compared to a benchmark material, which gave $S_{BET}$ = 1800 $m^2\ g^{-1}$ and $V_{micro}$ = 0.74 $cm^3\ g^{-1}$ (which corresponds to one of the highest porosity values described for this material)[25,26] the percentage of MOF is estimated to be about 2.1 wt% based on the composite microporous surface area. This value is in good agreement with the values deduced from elemental analysis results. The adsorption isotherms of pure $CO_2$, $N_2$, $O_2$, CO and $CH_4$ registered for evacuated composite samples were measured in the pressure range of 0–850 Torr at 298, 287 and 273 K, respectively. The single-component isotherms for each gas are shown in Fig. S18.† They exhibit good reversibility. $CO_2$

uptake shows a gradual increase with pressure with a higher slope than for other gases (Fig. S18a†). Such a nearly linear adsorption profile in the low pressure range has already been described for HKUST-1.[25,27,28] It reflects a strong preferential sorption of $CO_2$ with respect to other gases for this MOF. These results were confirmed by calculating sorption selectivities for $CO_2$ over CO, $CH_4$, $O_2$ and $N_2$ from the Henry constants, and by determining heats of adsorption of $CO_2$, CO and $CH_4$ (see ESI† for details). The potential of HKUST-1 to be used for selective $CO_2$/CO and $CO_2$/$CH_4$ separation in post- and pre-combustion capture technologies has been demonstrated.[27] Since the sorption properties of the HKUST-1 contained in membranes such as those described here are not altered as compared to the bulk material, these could be envisioned for designing separation devices for dedicated applications.

## Conclusions

A dynamic step-by-step procedure appears to be essential to achieve embedding of a crystalline coordination polymer such as HKUST-1 all over the length of the channels of a membrane. The fact that one of the reagents ([Cu(OAc)$_2$]$_2$ in the present case) is involved as a colloidal solution greatly improves the efficiency of this process. The formation of MOFs directly inside the channels offers several benefits: (i) the material synthesis and shaping are done in a single step; (ii) these composites are prepared at room temperature, using the very simple technique of flowing the reagents through the membrane; (iii) the MOF is protected by an inorganic-shell, and membranes are easy-to-handle objects (see Fig. S15†). Moreover, a selective embedding inside the channels is obtained when the membrane sides are coated with a metal-film such as Pt. Without the metal film, MOF crystals are grafted both on the external sides and inside the channels of the membranes. An increase in the amount of coordination polymer formed in the channels is certainly desirable. Further control over the MOF-coating homogeneity and thickness will possibly be reached by improving the anchorage on the channel surfaces through surface activation or SAM formation. Work in these directions, as well as experiments dedicated to the synthesis of other MOF composites, is currently under progress.

## Experimental section

### Materials

1,3,5-Benzenetricarboxylic acid (btc-$H_3$ in the following, Alfa Aesar, 98%), copper(II) nitrate (Cu(NO$_3$)$_2$·2.5H$_2$O, Aldrich, 98%) and copper(II) acetate (Cu(CH$_3$COO)$_2$·H$_2$O, Acros, 98%) were used without further purification. Absolute EtOH (99.9%, Sigma-Aldrich), 96% EtOH (Sigma-Aldrich) and deionized H$_2$O were employed as solvents. The CAAO membranes (200 nm) used are Whatman Anodisc 13 membranes.

Controlled flow-rate filtration was performed introducing the CAAO membranes in commercial Teflon filter-supports. Filtration flow-rates were controlled using programmable KDS-210 multichannel syringe pumps. To avoid the membrane occlusion by dust or non-dissolved reagents, the reagent
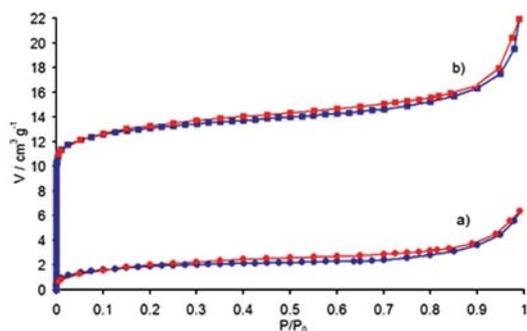


Fig. 5 $N_2$ adsorption isotherms recorded at 77 K for (a) pristine alumina membranes and (b) HKUST-1 loaded membranes.

solutions were systematically filtered through 200 nm Fluoropore membrane filters (Millipore). These filters were placed just before the Teflon supports holding the CAAO membranes. The A side of the membranes was systematically placed in such a way as to face the reagent flow (see ESI†).

## Characterizations

Infrared spectra (IR) were recorded with a Perkin-Elmer Spectrum 100 FT-IR spectrometer in the range of 600–4000 cm$^{-1}$. IR spectra were registered directly from composite membranes, except for the bulk reference material and for membranes resulting from solvothermal treatments (KBr pellets).

The powder X-ray diffraction (PXRD) patterns were collected on an Xpert pro (θ–θ mode) Panalytical diffractometer with λ ($Cu_{K\alpha 1}$, $Cu_{K\alpha 2}$) = 1.54059, 1.54439 Å.

The scanning electron microscopy (SEM) micrographs were taken with a JEOL JSM 6700F scanning electron microscope with a Field Emission Gun (FEG SEM). A thin layer of platinum was deposited on the samples to make them conductive. The time of metallization was 60 seconds and the current intensity was 80 mA.

Diffusion light scattering (DLS) measurements were performed on a Malvern Zetasizer 1000HS apparatus equipped with an argon laser (532 nm, 50 mW), a single-photon-counting avalanche photodiode for signal detection, and a digital autocorrelator. The colloidal solutions were systematically clarified by ultrafiltration through 200 nm Fluoropore membrane filters (Millipore). Measurements were performed in quartz cells of path length 10 mm that were transparent on all four sides, at a temperature regulated at 25.0 ± 0.1 °C and at a scattering angle of 90°. Data were interpreted with the non-negative least squares (NNLS) algorithm. For particle sizing in solution, the software gives multiple aspects and interpretations of the data collected for the sample, such as intensity, volume, and number distribution graphs as well as statistical analysis for each. The mean particle diameter is calculated by the software from the particle distributions measured, and the polydispersity index given is a measure of the size ranges present in the solution. A total of ten scans, each with a duration of 10 s, were accumulated for each analyzed sample. All the samples were analyzed in triplicate.

## Gas sorption measurements

20 pristine alumina membranes and 20 HKUST-1 loaded membranes obtained through dynamic SBS treatment of CAAO membranes with copper acetate colloids and btc-H$_3$ solutions were used for the measurements. They were broken in two/three pieces to allow their introduction in the measurement cell. Gas adsorption isotherms were performed on corresponding evacuated materials using the volumetric method with a Micromeritics ASAP 2010 or 2020 analyzer. Samples were previously warmed at 423 K under $10^{-5}$ Torr for at least 6 hours. The isotherms were recorded at equilibrium for several relative pressure values ($P/P_0$, $P_0$ = saturated vapor pressure) in a large range of $P/P_0$ ($10^{-7}$ to 1). The specific surface area were determined by physisorption of N$_2$ at 77 K using the standard BET method assuming a monolayer coverage of N$_2$ and a cross-sectional area of 16.2 Å$^2$ per molecule. For further information, see ESI.†

## CAAO membrane cleaning – Pt film deposition

CAAO membranes (bare or metallized) were systematically cleaned and degassed by immersion in boiling absolute ethanol (30 minutes), prior to air drying. A "CRESSINGTON 108 AUTO" sputter coater with a thickness controller "MTM20" was used to deposit 5 nm layers of Pt on both sides of the membranes engaged in the dynamic SBS approach.

## MOF@CAAO membrane by solvothermal synthesis

In a typical experiment, a cleaned and degassed CAAO membrane was placed in a home-made glass holder and introduced directly into the reaction mixture allowing the formation of bulk HKUST-1 (see ESI†). The CAAO substrates were held vertically, to avoid any precipitation by gravity on the membrane surface, and far enough from the reaction vessel bottom, to avoid them being shrouded in the bulk material. After the reaction as above, the membrane was thoroughly washed with water and ethanol, and dried in air. IR ($\nu$, cm$^{-1}$, KBr): $\nu$ = 730, 760, 1043, 1111, 1375, 1448, 1590, 1645 and 3430.

## MOF@CAAO membrane using static step-by-step synthesis

Two cleaned and degassed CAAO membranes were placed in a home-made glass holder which was dipped, in a cyclic fashion, in (a) a 1 mM (Cu(CH$_3$COO)$_2$·H$_2$O) solution in pure EtOH for 30 min, (b) pure EtOH for 15 min, (c) a 1 mM btc-H$_3$ solution in EtOH for 30 min, and (d) EtOH for 15 min. Immersions were performed at room temperature in solutions which were gently stirred with a magnetic rod. The first membrane was removed from the holder after 12 cycles, while 12 more cycles were applied on the remaining CAAO. After the final cycle, the CAAO membranes were thoroughly washed with EtOH and air dried. IR ($\nu$, cm$^{-1}$): $\nu$ = 1150, 1375, 1450, 1560, 1616, 1646 and 3400. Identical IR patterns were observed irrespective of the number of cycles applied on the metallized CAAO membrane.

## MOF@metallized CAAO membrane using dynamic step-by-step synthesis

**With absolute ethanol.** A 1 mM (Cu(CH$_3$COO)$_2$·H$_2$O) solution in absolute EtOH (30 min), absolute EtOH (15 min), a 1 mM btc-H$_3$ solution in absolute EtOH (30 min), and absolute EtOH (15 min) were allowed to flow, in a cyclic fashion, through a metallized CAAO membrane. The filtration flow rate was fixed at 0.5 mL min$^{-1}$. Once the desired number of cycles was applied on the substrate, the corresponding HKUST-1 composite membranes were thoroughly washed with EtOH and dried in air. IR ($\nu$, cm$^{-1}$): $\nu$ = 1150, 1375, 1450, 1560, 1616, 1646 and 3400. Identical IR patterns were observed irrespective of the number of cycles (2, 6, 12 and 24) applied on the metallized CAAO membrane.

**With 96% ethanol.** Copper acetate colloidal suspensions were obtained by dissolving (Cu(CH$_3$COO)$_2$·H$_2$O) (12 mg) in

96% EtOH (60 mL). Once filtered through a 200 nm Millipore filter, the resulting colloids present 40–60 nm copper acetate particles (see Fig. S12†). Neither sedimentation nor particle size modifications are observed when the evolution of the colloidal suspension is followed by DLS during several days.

Treatment of a metallized CAAO membrane by two cycles of the reagent sequence colloidal suspension (60 min), 96% EtOH (15 min), a 1 mM btc-$H_3$ solution in absolute EtOH (120 min), and absolute EtOH (15 min) afforded the desired composite membranes. IR ($\nu$, cm$^{-1}$): $\nu = 1150$, 1375, 1450, 1560, 1616, 1646 and 3400.

## Acknowledgements

## Notes and references

1 S. T. Meek, J. A. Greathouse and M. D. Allendorf, *Adv. Mater.*, 2011, **23**, 249–267.

2 A. Corma, H. Garcia and F. X. L. Xamena, *Chem. Rev.*, 2010, **110**, 4606–4655.

3 D. Farrusseng, S. Aguado and C. Pinel, *Angew. Chem., Int. Ed.*, 2009, **48**, 7502–7513.

4 L. J. Murray, M. Dinca and J. R. Long, *Chem. Soc. Rev.*, 2009, **38**, 1294–1314.

5 L. E. Kreno, K. Leong, O. K. Farha, M. Allendorf, R. P. Van Duyne and J. T. Hupp, *Chem. Rev.*, 2012, **112**, 1105–1125.

6 P. Horcajada, T. Chalati, C. Serre, B. Gillet, C. Sebrie, T. Baati, J. F. Eubank, D. Heurtaux, P. Clayette, C. Kreuz, J. S. Chang, Y. K. Hwang, V. Marsaud, P. N. Bories, L. Cynober, S. Gil, G. Ferey, P. Couvreur and R. Gref, *Nat. Mater.*, 2010, **9**, 172–178.

7 S. Hermes, F. Schroder, R. Chelmowski, C. Woll and R. A. Fischer, *J. Am. Chem. Soc.*, 2005, **127**, 13744–13745.

8 S. Mann, *Nature*, 1993, **365**, 499–505.

9 A. Bétard and R. A. Fischer, *Chem. Rev.*, 2012, **112**, 1055–1083.

10 O. Shekhah, J. Liu, R. A. Fischer and C. Woll, *Chem. Soc. Rev.*, 2011, **40**, 1081–1106.

11 A. Demessence, C. Boissiere, D. Grosso, P. Horcajada, C. Serre, G. Ferey, G. Soler-Illia and C. Sanchez, *J. Mater. Chem.*, 2010, **20**, 7676–7681.

12 Y. X. Hu, X. L. Dong, J. P. Nan, W. Q. Jin, X. M. Ren, N. P. Xu and Y. M. Lee, *Chem. Commun.*, 2011, **47**, 737–739.

13 M. D. Allendorf, R. J. T. Houk, L. Andruszkiewicz, A. A. Talin, J. Pikarsky, A. Choudhury, K. A. Gall and P. J. Hesketh, *J. Am. Chem. Soc.*, 2008, **130**, 14404–14405.

14 M. Rose, B. Bohringer, M. Jolly, R. Fischer and S. Kaskel, *Adv. Eng. Mater.*, 2011, **13**, 356–360.

15 E. V. Ramos-Fernandez, M. Garcia-Domingos, J. Juan-Alcaniz, J. Gascon and F. Kapteijn, *Appl. Catal., A*, 2011, **391**, 261–267.

16 M. Shah, M. C. McCarthy, S. Sachdeva, A. K. Lee and H. K. Jeong, *Ind. Eng. Chem. Res.*, 2012, **51**, 2179–2199.

17 D. Bradshaw, A. Garai and J. Huo, *Chem. Soc. Rev.*, 2012, **41**, 2344–2381.

18 P. Kuhn, J. Puigmarti-Luis, I. Imaz, D. Maspoch and P. S. Dittrich, *Lab Chip*, 2011, **11**, 753–757.

19 B. Platschek, A. Keilbach and T. Bein, *Adv. Mater.*, 2011, **23**, 2395–2412.

20 P. Ciambelli, L. Arurault, M. Sarno, S. Fontorbes, C. Leone, L. Datas, D. Sannino, P. Lenormand and S. Le Blond du Plouy, *Nanotechnology*, 2011, **22**, 265613, (12p).

21 S. Aguado, J. Canivet and D. Farrusseng, *J. Mater. Chem.*, 2011, **21**, 7582–7588.

22 S. S. Y. Chui, S. M. F. Lo, J. P. H. Charmant, A. G. Orpen and I. D. Williams, *Science*, 1999, **283**, 1148–1150.

23 D. Mustafa, E. Breynaert, S. R. Bajpe, J. A. Martens and C. E. A. Kirschhock, *Chem. Commun.*, 2011, **47**, 8037–8039.

24 K. S. W. Sing, D. H. Everett, R. A. W. Haul, L. Moscou, R. A. Pierotti, J. Rouquerol and T. Siemieniewska, *Pure Appl. Chem.*, 1985, **57**, 603–619.

25 P. Chowdhury, C. Bikkina, D. Meister, F. Dreisbach and S. Gumma, *Microporous Mesoporous Mater.*, 2009, **117**, 406–413.

26 Y.-K. Seo, G. Hundal, I. T. Jang, Y. K. Hwang, C.-H. Jun and J.-S. Chang, *Microporous Mesoporous Mater.*, 2009, **119**, 331–337.

27 Q. M. Wang, D. M. Shen, M. Bulow, M. L. Lau, S. G. Deng, F. R. Fitch, N. O. Lemcoff and J. Semanscin, *Microporous Mesoporous Mater.*, 2002, **55**, 217–230.

28 P. Chowdhury, S. Mekala, F. Dreisbach and S. Gumma, *Microporous Mesoporous Mater.*, 2012, **152**, 246–252.